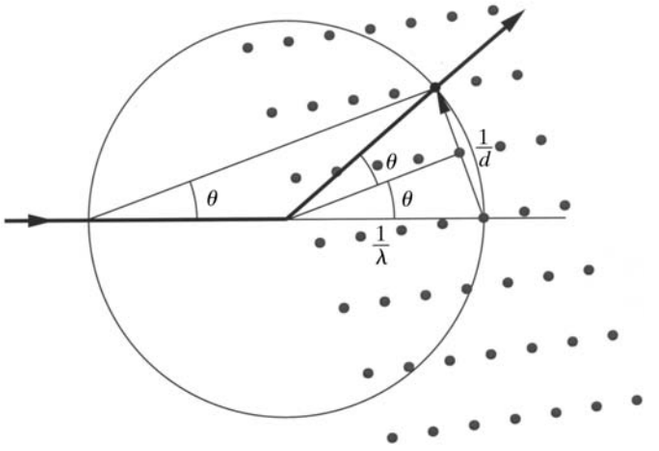

Figure 9.1.6.1
The Ewald-sphere construction. A reciprocal-lattice point lies on the surface of the sphere if the following trigonometric condition is fulfilled: $1/2d = (1/\lambda)\sin\theta$. After a simple rearrangement, it takes the form of Bragg's law: $\lambda = 2d\sin\theta$. Therefore, when a reciprocal-lattice point with indices *hkl* lies on the surface of the Ewald sphere, the interference condition for that particular reflection is fulfilled and it gives rise to a diffracted beam directed along the line joining the centre of the sphere to the reciprocal-lattice point on the surface.

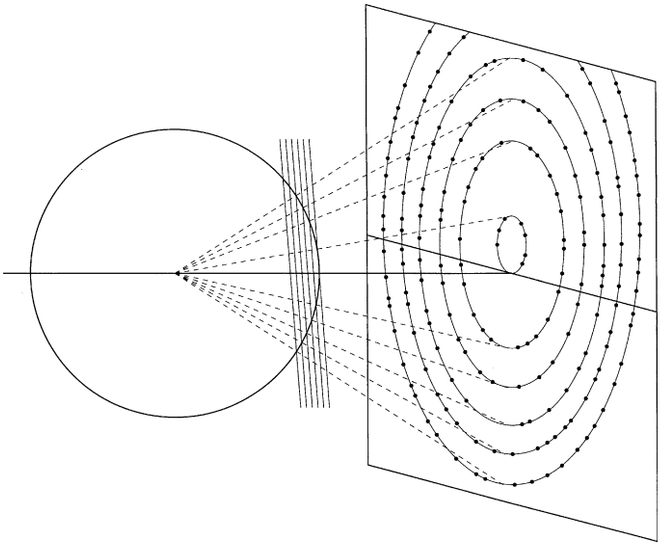

Figure 9.1.6.2
The plane of reflections in the reciprocal sphere that is approximately perpendicular to the X-ray beam gives rise to an ellipse of reflections on the detector.

recorded in minutes rather than hours and has transformed approaches to data collection.

While the CCD has revolutionized data-collection times, further advances are expected from the use of solid-state pixel detectors. Such detectors record individual X-ray quanta and have essentially zero read-out time. The most advanced of these, the PILATUS 1M device, is a hybrid pixel array detector (Broennimann *et al.*, 2006; Hülsen *et al.*, 2006), first installed at the Swiss Light Source.

Almost all current 2D detectors are used in conjunction with a goniostat, providing rotation of the crystal about a single axis during exposure. Indeed, the majority of instruments have only a single rotation axis. The remainder are based on the kappa (ω, κ, φ) cradle to select different initial orientations of the sample in the beam; the sample is nevertheless subsequently rotated about a single axis for data collection.

9.1.6. Basis of the rotation method

9.1.6.1. Rotation geometry

The physical process of diffraction from a crystal involves the interference of X-rays scattered from the electron clouds around the atomic centres. The ordered repetition of atomic positions in all unit cells leads to discrete peaks in the diffraction pattern. The geometry of this process can alternatively be described as resulting from the reflection of X-rays from a set of hypothetical planes in the crystal. This is explained by the Ewald construction (Fig. 9.1.6.1), which provides a visualization of Bragg's law. Monochromatic radiation is represented by a sphere of radius $1/\lambda$, and the crystal by a reciprocal lattice. The lattice consists of points lying at the end of vectors normal to reflecting planes, with a length inversely proportional to the interplanar spacing, $1/d$. In the rotation method, the crystal is rotated about a single axis, with the rotation angle defined as φ. A seminal work, giving an excellent background to this field by a number of contributors, was edited by Arndt & Wonacott (1977). A more recent review of the method is provided by Dauter (2005).

9.1.6.2. Diffraction pattern at a single orientation: the 'still' image

For a stationary crystal in any particular orientation (a so-called 'still' exposure), only a fraction of the total number of Bragg reflections will satisfy the diffracting condition. The number of reflections will be very limited for a small-molecule crystal, possibly zero in some orientations. Macromolecules have large unit cells, of the order of 100 Å, compared with the wavelength of the radiation, which is about 1.0 Å. In geometric terms, the reciprocal space is densely populated with points in relation to the size of the Ewald sphere. Thus, more reflections diffract simultaneously but at different angles, since many reciprocal-lattice points (reflections) lie simultaneously on the surface of the Ewald sphere in any crystal orientation. This is the great advantage of 2D detectors for large cell dimensions.

The real crystal is a regular and ordered array of unit cells. This means that reciprocal space is made up of a set of points organized in regular planes. For a still exposure, any particular plane of points in the reciprocal lattice intersects the surface of the Ewald sphere in the form of a circle. The corresponding diffracted rays, originating from the centre of the Ewald sphere, form a cone that intersects the sphere on the circle formed by the set of points. In most experiments, the detector is placed perpendicular to the direct beam and the cone of diffracted rays forms an ellipse of spots on its surface (Fig. 9.1.6.2). If a major axis of the crystal lies nearly parallel to the beam, then the ellipses will approximate a set of circles around the centre of the detector. All reflections within each circle will have one index in common, corresponding to the unit-cell axis lying along the beam. For non-centred unit cells, this index will increase by one in successive circles. The gaps between the circles depend on the spacing between the members of the set of reciprocal-lattice planes and are inversely proportional to the real cell dimension related to these planes.

Still exposures were used extensively in the early applications of the rotation method for estimation of crystal alignment. The geometric location of the spots with respect to the origin allows accurate determination of the unit-cell parameters and the crystal orientation. This approach has been superseded in modern

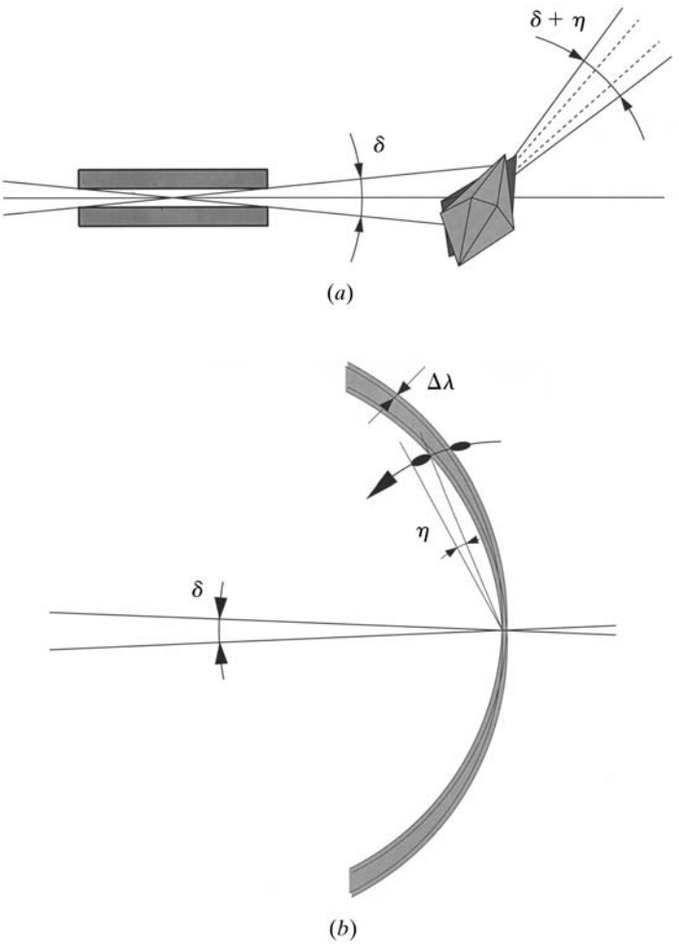

Figure 9.1.6.3
Schematic representation of beam divergence (δ) and crystal mosaicity (η). (*a*) In direct space, (*b*) in reciprocal space, where the additional thickness of the Ewald sphere results from the finite wavelength bandpass, $\delta\lambda/\lambda$.

software packages by autoindexing algorithms using real rotation images.

9.1.6.3. Rocking curve: crystal mosaicity and beam divergence

The Ewald-sphere construction assumes an ideal source with a totally parallel X-ray beam and an ideal crystal with all unit cells having identical relative orientation, resulting in infinitely sharp Bragg reflections. These assumptions lead to a sphere of radius $1/\lambda$ attached rigidly to the beam and with the crystal in a particular orientation as a reciprocal lattice consisting of mathematical points. A real experiment deviates from this in three respects. Firstly, the incident beam is not strictly parallel. On a conventional rotating-anode source the beam can only be focused and collimated to be parallel within a small angle, with a divergence of about 0.2° (with mirror optics) and 0.4° (with a monochromator). On SR sources, a much smaller beam divergence can be achieved, and, indeed, beamlines on third-generation SR sources approach the ideal ever more closely. The horizontal and vertical beam divergence may differ, and this must be taken into account. The Ewald sphere now has two limiting orientations which result in a nonzero active width. Secondly, the X-radiation is only monochromatic within a defined wavelength bandpass, $\delta\lambda/\lambda$, of the order 0.0002–0.001 at synchrotron beamlines, but considerably more for laboratory sources. The wavelength bandpass, in effect, thickens the surface of the Ewald sphere. Thirdly, real crystals are made up of small mosaic blocks imperfectly oriented relative to one another, increasing the total rocking curve. At room temperature, protein crystals often show a mosaic spread less than 0.05°, but for some samples this may be much larger. However, vitrification of crystals in many cases leads to substantial increase of mosaicity to sometimes more than 1°. In the reciprocal lattice, the effect of this is to give a finite dimension to each of the lattice points.

These effects are schematically illustrated in Fig. 9.1.6.3. The combined result is that the diffraction of a particular reflection is spread over a range of crystal rotation.

9.1.6.4. Rotation images and lunes

Using monochromatic radiation, in order to measure the remaining reflections that do not lie on the surface of the sphere, the crystal must be rotated to bring the reflections into the diffracting condition. If the crystal is rotated about a single axis during sequential exposures, this is known as the rotation method. The rotation axis is, in practice, chosen to be perpendicular to the beam to preserve the symmetry between the two halves of the complete pattern. This is the most commonly applied method of data collection for macromolecular crystals (Arndt & Wonacott, 1977).

If the crystal is rotated during exposure, the ellipses observed on a still image change their position on the detector. In effect, all reflections diffracting during one exposure will be contained within lunes formed between the two limiting positions of each ellipse at the start and end of the given rotation. The width of the lunes in the direction of the crystal rotation, perpendicular to the rotation axis, is proportional to the rotation range per exposure. In contrast, along the rotation axis the width of the lunes is very small, since the intersection of the reciprocal-lattice plane with the Ewald sphere does not change significantly. For crystals of small molecules, the lunes are not pronounced, owing to the sparse population of reciprocal space, but for crystals with large cell dimensions, the lunes are densely populated by diffraction spots and often exhibit clear and well pronounced edges. At high resolution, the mapping of the reciprocal lattice within each lune is distorted, and rows of reflections form hyperbolas. At low diffraction angles, where the surface of the Ewald sphere is approximately flat, this distortion is minimal, and the lunes look like fragments of precession photographs.

9.1.6.5. Partially and fully recorded reflections

The rotation method gives rise to lunes of data between the ellipses that relate to the start and the end of the rotation range used for the exposure. The data are complete if the Ewald sphere has been crossed by all reflections in the asymmetric part of the reciprocal lattice, which means that the crystal has to be rotated in total by a substantial angle. However, it is impossible to record all the data in a single exposure with such a wide rotation, owing to overlapping of the diffraction spots.

In practical applications to macromolecules, the total rotation is divided into a series of narrow individual rotations of width $\Delta\varphi$. In each of these, the crystal is exposed for a specified time or X-ray dose per angular unit. Each reflection diffracts over a defined crystal rotation and hence time interval, owing to the finite value of the rocking curve or angular spread, here referred to as ξ, the combined effect of beam divergence (δ) and crystal mosaicity (η). Provided ξ is less than $\Delta\varphi$, some reflections will start and finish crossing the Ewald sphere and hence diffract within one exposure. Their full intensity will be recorded on a

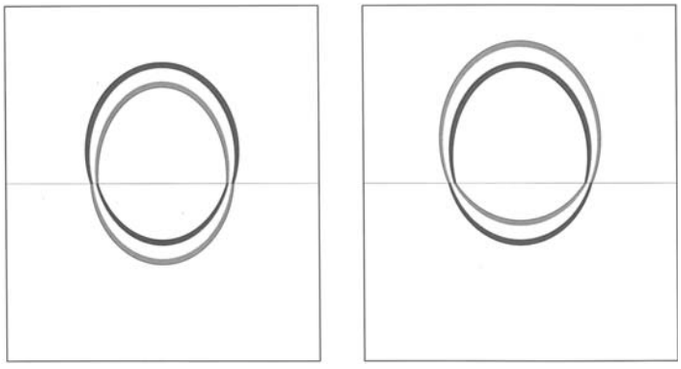

Figure 9.1.6.4
A single lune on two consecutive exposures. The partial reflections appear on both images and their intensity is distributed over both.

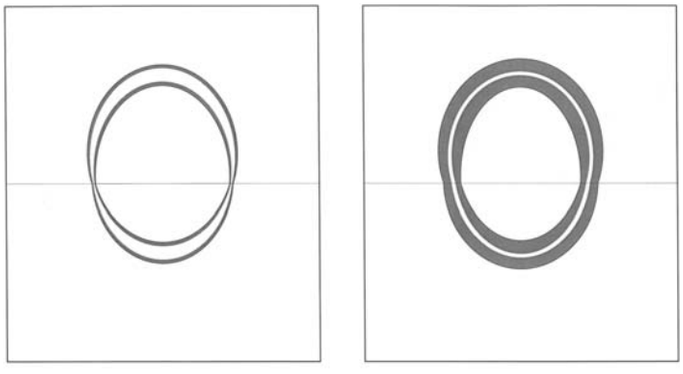

Figure 9.1.6.5
Appearance of a lune for (left) a crystal of low mosaicity and (right) a highly mosaic crystal. Characteristically, the width of the lune along the rotation axis is wider if the mosaicity is high.

single image, and these are referred to as fully recorded reflections, or fullys.

Other reflections will start to diffract during one exposure, but will still be diffracting at the end of the $\Delta\varphi$ rotation range. The remaining intensity of these reflections will be recorded on subsequent images. There will of course be corresponding reflections at the start of the present image. These reflections are termed partially recorded, or partials. Fig. 9.1.6.4 shows schematically how a lune appears on two consecutive exposures, with partials at each edge. The partials at the bottom edge of each lune contain the rest of the intensity of the partials from the previous exposure. The rest of the intensity of the partials at the top of the lune will appear on the next exposure. Superposition of two successive images will reveal some spots common to both: they are the partials shared between the two. If the angular spread ξ is small compared with the rotation range $\Delta\varphi$ then most reflections will be fully recorded. As ξ increases, the proportion of partials will rise, and when it reaches or exceeds $\Delta\varphi$ in magnitude there will be no fully recorded reflections. If the rotation range per image is small compared with the rocking curve, individual reflections can be spread over several images.

As ξ increases, the lunes become wider (Fig. 9.1.6.5), since there are more partial reflections crossing the Ewald sphere at any one time. The appearance of the lunes can be used to estimate the mosaicity of the crystal. If the edges are sharply defined, then the mosaicity is low. In contrast, if the intensities at the edges gradually fade away, then the mosaicity must be high. Indeed, this phenomenon can be exploited by the integration software to provide accurate definition of the orientation parameters and of the mosaicity.

A key characteristic of high mosaicity is that all lunes are wide in the region along the rotation axis. On still exposures, the width of the rings is proportional to the angular spread. The width of lunes is expected to be very small along the rotation axis. If they are wide in this region, this is especially indicative of high mosaic spread. While highly ordered crystals with low mosaicity are preferable and often lead to data of the highest quality, high mosaic spread is not a prohibitive factor in accurate intensity estimation, provided it is properly taken into account in estimating the data collection and integration parameters, such as individual rotation ranges.

9.1.6.6. The width of the rotation range per image: fine φ slicing

An important variable in the rotation method is the width of the rotation ranges per individual exposure. The two basic approaches can be termed wide and fine φ slicing, and differ in the relation between the angular spread and the rotation range per exposure. The two methods are applicable under different experimental constraints.

Fine φ slicing requires that the individual intensities are divided over several consecutive images, *i.e.* $\Delta\varphi$ should be substantially less than ξ (Kabsch, 1988). This approach possesses two very positive features. Firstly, it minimizes the background by integrating intensities only over a φ range equivalent to the rocking curve of the crystal. Secondly, it allows the fitting of 3D profiles to the pixels that compose a reflection, the first two dimensions being the *xy* plane of the detector and the third the φ rotation. In combination, these should provide an optimum signal-to-noise ratio for the measured intensities and would appear to be the method of choice for data collection.

However, this involves a very large number of images, which can pose logistical problems in terms of data handling. Only if the read-out time is negligible in comparison with the exposure time can fine slicing be applied. If the detector read-out is slow, fine slicing becomes totally impractical. Multiwire chambers allow fine φ slicing, but unfortunately their disadvantages in terms of effective dynamic range preclude their use on high-intensity sources. Imaging plates are generally too slow for this approach.

The fine-slicing method is likely to receive a resurgence of interest with the introduction of fast read-out detectors such as the PILATUS, where diffraction images can be acquired continuously without the use of a beam shutter (Hülsen *et al.*, 2006).

9.1.6.7. Wide slicing

The object of the wide-slicing approach is to acquire the data on as small a number of individual exposures as possible. It involves large $\Delta\varphi$ values per image, usually of the order of 0.5° or more, which exceed the angular spread. Each image contains a considerable proportion of fully recorded reflections. Originally, wide slicing was used to minimize the large numbers of X-ray films to be processed. Only the wide-slicing approach is tractable for detector systems where the read-out time is relatively slow in relation to exposure, *e.g.* imaging plates with read-out times of 20 seconds to minutes.

Wide slicing has two drawbacks. Firstly, during integration of the intensity data, only 2D profiles are fitted for each individual spot in the wide slicing. Secondly, each reflection profile overlaps a background which accumulates throughout the whole time and

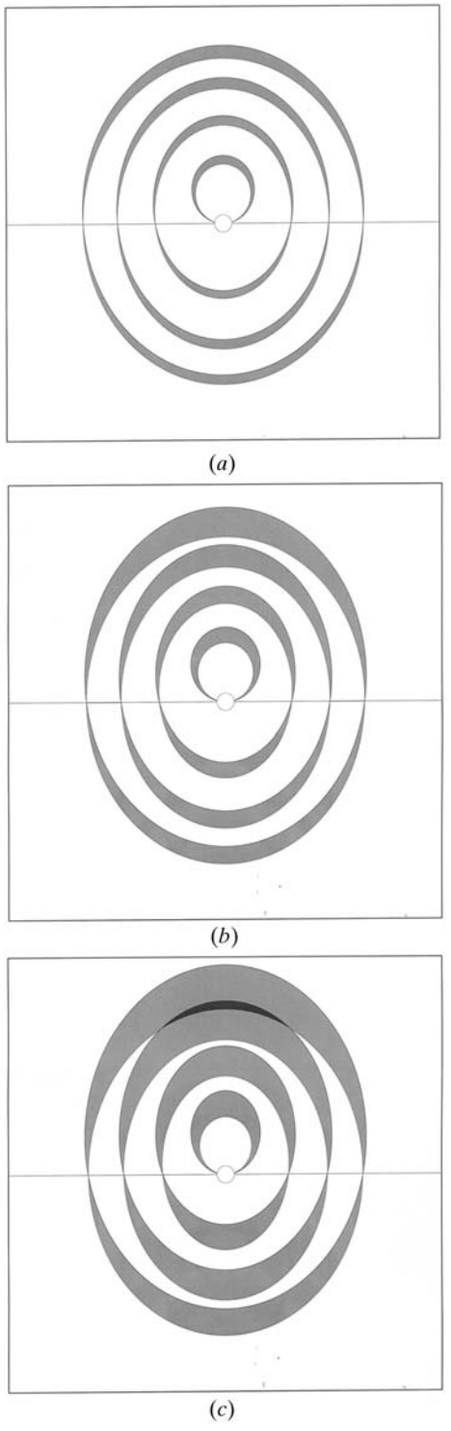

Figure 9.1.6.6
The width of the lunes is proportional to the rotation range per image, $\Delta\varphi$, which increases from (*a*) to (*c*). If the rotation range is large, the lunes overlap at high resolution.

angular range of the exposure, even when the reflection concerned is not diffracting.

The aim is to use the maximum acceptable rotation range per image. The lunes on an image have a finite width proportional to the rotation range. This width restricts the allowed angular range per image, as overlap of spots resulting from overlap of adjacent lunes must be avoided if the intensities are to be successfully integrated (Fig. 9.1.6.6). Several factors affect the degree of overlap and will be discussed in the rest of this section. A simple formula (Fig. 9.1.6.7) can be used to estimate the maximum permitted rotation range per image:

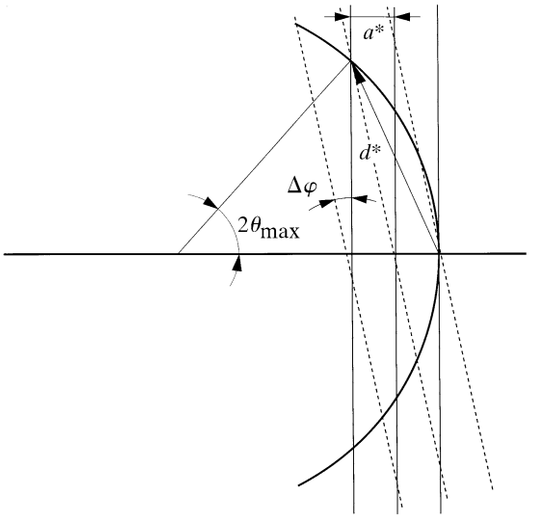

Figure 9.1.6.7
The largest allowed rotation range per exposure depends on the dimension of the primitive unit cell oriented along the X-ray beam; this is diminished by high mosaicity.

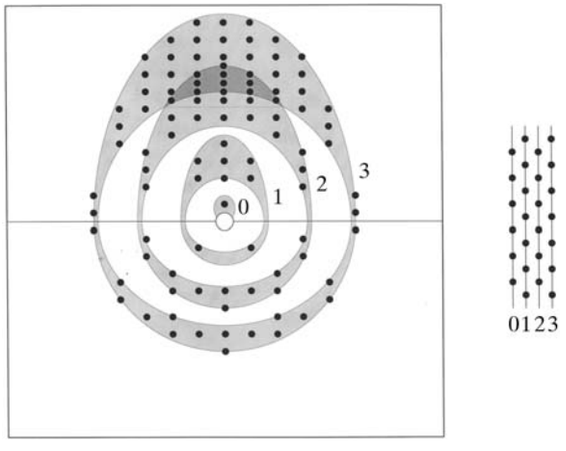

Figure 9.1.6.8
If the crystal lattice is centred or if its orientation is non-axial, the reflections do not overlap in spite of overlapping lunes, as illustrated on the right with consecutive layers of reflections viewed from the side.

$$\Delta\varphi = 180d/\pi a - \xi,$$

where the factor $180/\pi$ converts radians to degrees, ξ is the angular spread of the reflection, d is the high-resolution limit and a is the length of the primitive cell dimension along the direction of the X-ray beam. However, this simplistic equation can be somewhat misleading. It most strictly applies when the lunes are densely packed with reflections, for an orthogonal cell rotated about a major axis. If this is not the case, then often rows of reflections from one lune fit between rows in the adjacent lune without overlap. For example, for a trigonal crystal with its a axis along the beam and rotating about its c axis, even and odd lunes contain rows of reflections that lie between one another on the detector (Fig. 9.1.6.8).

It can be extremely hard to record data from samples with a very long cell dimension. If the long axis lies along the X-ray beam, then it will restrict $\Delta\varphi$ considerably to very low values. This is exacerbated if the mosaicity is substantial. It is therefore beneficial to have the longest axis oriented roughly along the

spindle axis, as it can then never lie parallel to the beam. This can be a problem with cryogenic samples mounted in loops, where the preferred orientation is hard to dictate, and this is an example where a κ-goniostat is an advantage, allowing reorientation of the crystal.

Simplistic application of the above equation for estimating $\Delta\varphi$ is not receommended. The degree of overlap also depends on pixel size, beam cross section, crystal size and mosaicity, and crystal-to-detector distance. Given the influence of these additional parameters, it is in practice better to employ the integration software first to interpret the diffraction pattern and to simulate predicted patterns by adjusting the data-collection parameters. Several modern packages have such strategy features, and it is vital to employ them before collecting data. In fact, from a theoretical point of view, the highest signal-to-noise ratio is obtained when $\Delta\varphi$ corresponds to the rocking curve of the diffraction, *i.e.* the mosaic spread plus the beam divergence.

9.1.7. Rotation method: geometrical completeness

This topic has been reviewed by Dauter (2005).

9.1.7.1. Total rotation range for non-anomalous data

The total set of structure-factor amplitudes from a crystal is a sphere of points in reciprocal space, with a radius defined by the maximum resolution. The intensities of the two hemispheres of data show a centrosymmetric relationship based on Friedel's law, which only breaks down if anomalous scatterers are present. However, the diffraction pattern possesses internal symmetry related to that of the real-space unit cell. This means that for all space groups an asymmetric unit of reciprocal space can be defined. Provided the intensities of all reflections in this asymmetric unit have been measured, those of all others can be generated by the symmetry operations and the Fourier transform for the complete structure computed.

The asymmetric unit has the shape of a wedge extending from the origin at the centre of the reciprocal sphere with a cutoff at a maximum radius corresponding to the limiting diffraction angle (resolution). Once the Laue symmetry group of the crystal has been determined (*International Tables for Crystallography*, Volume A, 2005), it is straightforward to define the shape of this wedge and establish which data must be recorded to make up a complete unique set. For macromolecular crystals, where there can be no centre of symmetry, the possibilities are further simplified to the point group rather than the Laue group. All space groups belonging to the same point group have the same asymmetric unit. The only differences lie in the presence or absence of screw axes or centring. Thus, space groups $P2_12_12_1$, $P2_12_12$, $P222_1$, $P222$, $I222$ and $I2_12_12_1$ all belong to point group (symmetry class) 222 and have the same asymmetric unit in reciprocal space. The only consequence of the presence of screw axes or lattice centring is to introduce systematic absences for some classes of reflection within this asymmetric unit of the point group.

It is usual to define the limits of the asymmetric unit by placing restrictions on the indices. For point group 222, the common conventional choice of limits on the reflection indices hkl is

$$0 \le h \le h_{\max}, \qquad 0 \le k \le k_{\max} \qquad 0 \le l \le l_{\max},$$

where $h_{\max}$, $k_{\max}$ and $l_{\max}$ are defined by the maximum resolution. In all point groups, there are multiple but equivalent ways of defining the asymmetric unit, but a default definition is generally chosen by the data-reduction software. For example, in triclinic symmetry, any hemisphere constitutes an asymmetric unit, and there are three typical choices of index limits:

$$0 \le h \le h_{\max}, \qquad \bar{k}_{\min} \le k \le k_{\max}, \qquad \bar{l}_{\min} \le l \le l_{\max},$$

or

$$\bar{h}_{\min} \le h \le h_{\max}, \qquad 0 \le k \le k_{\max}, \qquad \bar{l}_{\min} \le l \le l_{\max},$$

or

$$\bar{h}_{\min} \le h \le h_{\max}, \qquad \bar{k}_{\min} \le k \le k_{\max}, \qquad 0 \le l \le l_{\max}.$$

The standard choices of asymmetric unit taken from the *CCP*4 program suite (Collaborative Computational Project Number 4, 1994) are shown in Table 9.1.7.1.

The data are complete if the Ewald sphere has been crossed by all reflections in the asymmetric part of the reciprocal lattice. During data acquisition and reduction, all measured indices are conventionally transformed to this asymmetric unit of reciprocal space. Firstly, this allows merging of symmetry-equivalent measurements as appropriate. Secondly, it allows the completeness of the data to be assessed efficiently, using contributions from the whole sphere.

For all point groups, rotation of the crystal by 180° from any starting angle on the φ spindle axis is sufficient to provide a complete set of data (this is not sufficient if anomalous-dispersion measurements are required; see Section 9.1.7.2). Given such a total rotation, the redundancy of the measurements will increase with higher crystal symmetry. Thus, for a triclinic space group, the unique data will be measured almost twice on average (see the blind region below); for orthorhombic, eight times; for hexagonal class 6, 12 times; and for 622, 24 times. Redundancy is, in principle, advantageous, giving improved data quality (again see below), but it is generally possible to record complete unique data with a minimal overall rotation and correctly chosen starting angle on the spindle. It is of course necessary to determine the crystal orientation matrix, and this remains a vital part of the data-collection strategy. To minimize the effects of radiation

Table 9.1.7.1
Standard choice of asymmetric unit in reciprocal space for different point groups from the *CCP4* program suite

Point group	Index limits	
1	hkl: $hk0$: $0k0$:	$l \ge 0$ $h \ge 0$ $k \ge 0$
2	hkl: $hk0$:	$k \ge 0, l \ge 0$ $h \ge 0$
222	hkl:	$h \ge 0, k \ge 0, l \ge 0$
4	hkl: $0kl$:	$h \ge 0, k > 0, l \ge 0$ $k \ge 0$
422	hkl:	$h \ge k, k \ge 0, l \ge 0$
3	hkl: $00l$:	$h \ge 0, k > 0$ $l > 0$
321	hkl: hhl:	$h \ge k, k \ge 0$ $l \ge 0$
312	hkl: $h0l$:	$h \ge k, k \ge 0$ $l \ge 0$
6	hkl: $0kl$:	$h \ge 0, k > 0, l \ge 0$ $k \ge 0$
622	hkl:	$h \ge k, k \ge 0, l \ge 0$
23	hkl: hkh:	$h \ge 0, k > h, l > h$ $k \ge h$
432	hkl:	$h \ge 0, k \ge l, l \ge h$